Exploring the thermally-controlled fentanyl transdermal therapy to provide constant drug delivery by physics-based digital twins

Flora Bahrami , Agnes Psikuta , René Michel Rossi , Alex Dommann , Thijs Defraeye

PII: S0928-0987(24)00160-X
DOI: https://doi.org/10.1016/j.ejps.2024.106848
Reference: PHASCI 106848

To appear in: *European Journal of Pharmaceutical Sciences*

Received date: 5 April 2024
Revised date: 20 June 2024
Accepted date: 7 July 2024

Please cite this article as: Flora Bahrami , Agnes Psikuta , René Michel Rossi , Alex Dommann , Thijs Defraeye , Exploring the thermally-controlled fentanyl transdermal therapy to provide constant drug delivery by physics-based digital twins, *European Journal of Pharmaceutical Sciences* (2024), doi: https://doi.org/10.1016/j.ejps.2024.106848

Exploring the thermally-controlled fentanyl transdermal therapy to provide constant drug delivery by physics-based digital twins

Flora Bahrami [1,2], Agnes Psikuta[1], René Michel Rossi [1], Alex Dommann [2], Thijs Defraeye [1,*]

[1] Empa, Swiss Federal Laboratories for Materials Science and Technology, Laboratory for Biomimetic Membranes and Textiles, Lerchenfeldstrasse 5, CH-9014 St. Gallen, Switzerland

[2] University of Bern, ARTORG Center for Biomedical Engineering Research, Mittelstrasse 43, CH-3012 Bern, Switzerland

Abstract

Transdermal drug delivery is suitable for low-molecular-weight drugs with specific lipophilicity, like fentanyl, which is widely used for cancer-induced pain management. However, fentanyl's transdermal therapy displays high intra-individual variability. Factors like skin characteristics at application sites and ambient temperature contribute to this variation. In this study, we developed a physics-based digital twin of the human body to cope with this variability and propose better adapted setups. This twin includes an *in-silico* skin model for drug penetration, a pharmacokinetic model, and a pharmacodynamic model. Based on the results of our simulations, applying the patch on the flank (side abdominal area) showed a 15.3% higher maximum fentanyl concentration in the plasma than on the chest. Additionally, the time to reach this maximum concentration when delivered through the flank was 19.8 h, which was 10.3 h earlier than via the upper arm. Finally, this variation led to an 18% lower minimum pain intensity for delivery via the flank than the chest. Moreover, the impact of seasonal changes on ambient temperature and skin temperature by considering the activity level was investigated. Based on our result, the fentanyl uptake flux by capillaries increased by up to 11.8% from an inactive state in winter to an active state in summer. We also evaluated the effect of controlling fentanyl delivery by adjusting the temperature of the patch to alleviate the pain to reach a mild pain intensity (rated three on the VAS scale). By implementing this strategy, the average pain intensity decreased by 1.1 points, and the standard deviation for fentanyl concentration in plasma and average pain intensity reduced by 37.5% and 33.3%, respectively. Therefore, our digital twin demonstrated the efficacy of controlled drug release through temperature regulation, ensuring the therapy toward the intended target outcome and reducing therapy outcome variability. This holds promise as a potentially useful tool for physicians.

Corresponding author:
Thijs Defraeye, thijs.defraeye@empa.ch

1 Introduction

The transdermal delivery system administers drugs through the skin to the body, the largest and outermost organ in the human body [1]. Transdermal delivery offers benefits, including less fluctuation in drug intake, bypassing first-pass metabolism, and enhancing patient compliance [2]. On the other hand, it has limitations, such as it is only suitable for low molecular weight potent drugs [3]. Fentanyl is one of the common drugs administrated transdermally. It is a synthetic opioid that is 50 to 100 times more potent than morphine [4] and commonly used as an analgesic for cancer-induced pain [5]. However, fentanyl transdermal therapy shows intra and inter-individual variability [6]. This implies that fentanyl transdermal therapy leads to different outcomes among patients and even for each patient during the treatment. Various factors contribute to the variability in outcomes following the application of a fentanyl patch. These include differences in skin characteristics at the different application sites on the human body [7–9], skin temperature [10,11] and age, weight, and gender [12]. However, the task of fine-tuning the fentanyl dosage for each patient by trial and error is currently the only way to go, despite the mentioned drawbacks.

As a future improvement, computational and mathematical methods could be employed to personalize and adapt transdermal therapy for patients while reducing clinical trial and error methods, which are costly and might put the patient's health and well-being at risk. Some of these computational methods aim to monitor fentanyl penetration through the skin via molecular dynamics models [13–15], brick-and-mortar models [16], or diffusion models [9,17–23] with numerical and analytical solutions. Additionally, other computational methods focus on the pharmacokinetics and pharmacodynamics model, which aim to predict the drug concentration in plasma by considering the metabolism and eliminations and, eventually, the drug's effect corresponding to the drug concentration [21,22,24–27]. These models can contribute to evaluating the impact and efficacy of new delivery technologies, such as microneedles [28,29], iontophoresis [30,31], or the application of heat to steer transdermal drug delivery [32,33]. Furthermore, some studies explored *in-silico* the impact of anatomical sites on fentanyl delivery [9]. Also, physics-based digital twins of the human body were developed by combining the transdermal uptake through the *in-silico* model of skin with pharmacokinetics and pharmacodynamics models in order to predict and modify the fentanyl transdermal therapy for virtual patients based on their physiological features and response to the therapy for entire populations of patients [21,22]. However, these virtual twins of patients for fentanyl therapy have not been used to investigate *in-silico* the impact of novel technologies, such as microneedles, or the impact of thermally-controlled delivery.

In this study, we applied the digital human twin for thermally controlling the fentanyl flux to the body to keep the outcome of the treatment in the acceptable range. For this purpose, we developed a digital twin that includes drug uptake through the *in-silico* skin model, pharmacokinetic, and pharmacodynamic models. For monitoring the drug penetration from the patch through the skin, we developed a new model including different layers of the skin, i.e., stratum corneum, viable epidermis, dermal papillae, dermis, hypodermis, and capillary vessels, to simulate blood flow. Additionally, we took into account the changes in the properties of the skin as the virtual patient implemented the patch on different body sites, including the chest, back, flank, and upper arm. Furthermore, the impact of seasonal changes on the ambient temperature by considering the activity state of the patient on the fentanyl uptake by the skin was studied. In the end, we implemented this temperature dependency of fentanyl penetration in order to steer fentanyl flux to the body in order to control fentanyl concentration in the plasma and, eventually, the pain intensity of the patient.

2 Materials and methods

The general approach of this study is to develop a virtual human twin for transdermal therapy, which includes three main blocks of drug uptake, pharmacokinetics, and pharmacodynamics model. To do so, we developed a detailed *in-silico* model of skin, which, besides considering the stratum corneum, viable epidermis, dermis, and hypodermis, includes dermal papillae and capillary networks. Later, this model was used to predict the uptake of fentanyl from the patch by using Fick's second law and blood flow in the capillaries. Additionally, the Pharmacokinetics model calculates the fentanyl concentration in plasma based on the flux of fentanyl uptake to blood circulation, drug distribution, metabolism, and elimination. Based on the calculated fentanyl concentration in the plasma, the pharmacodynamics model calculates the effect of fentanyl therapy, which is pain relief. Furthermore, within the developed digital twin, we explored the changes in the skin layers in different body sites, such as the chest, back, and upper arm, to evaluate the variation in the therapy outcome between each patch administration. Moreover, we took into account how the ambient temperature of the room the patient resides in affects the fentanyl uptake by considering summer and winter conditions. Later on, we took a step further to implement the impact of heat on fentanyl uptake in order to provide heat-enhanced fentanyl delivery to control the fentanyl concentration and, subsequently, pain intensity in a target range. The overall structure of this study is provided in Figure 1.

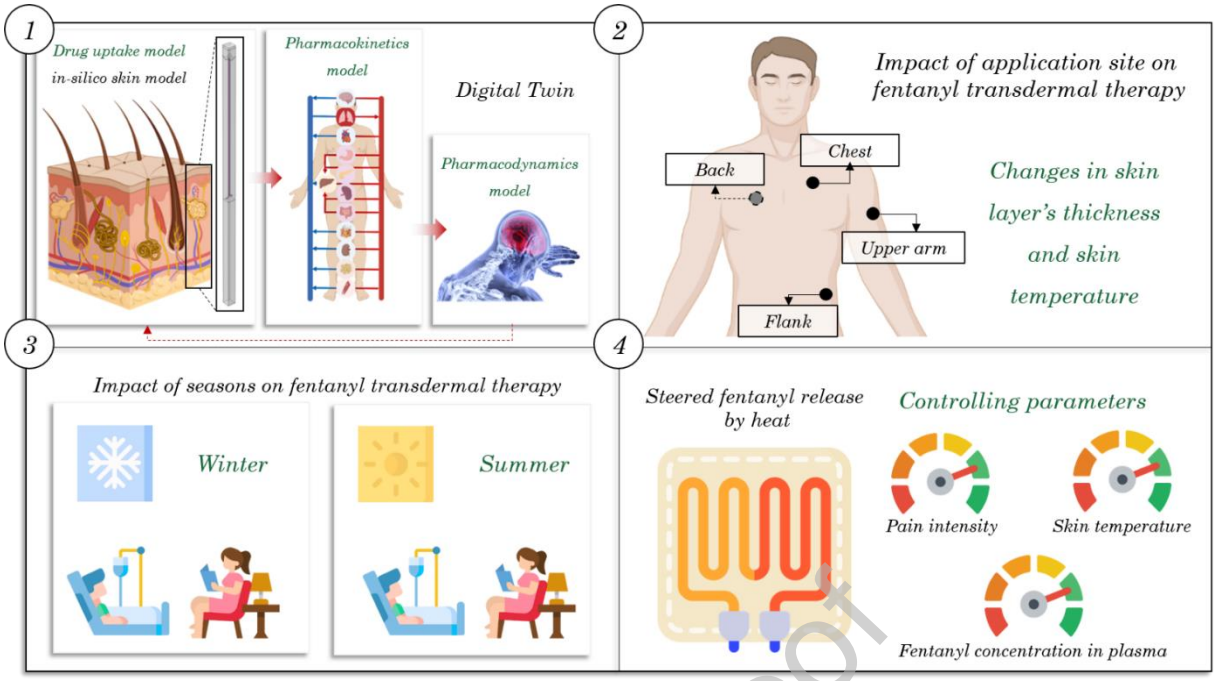

Figure 1- The overall structure of this study, which takes into account a detailed structure of the skin, the impact of body sites on drug uptake, the impact of ambient temperature on drug uptake, and finally, heat-enhanced delivery to control pain management therapy. (Created with elements from BioRender.com and www.flaticon.com)

2.1 Digital twin

2.1.1 Drug uptake model for the skin

2.1.1.1 Geometry

The geometry involved in the drug uptake model includes a patch, stratum corneum, viable epidermis, and dermal papillae, which provide a curved interface between the epidermis and dermis, dermis, capillary vessels, and hypodermis, which is shown in Figure 2. it should be noted for simplification the arterial capillary is connected directly to the venous capillary; however, the drug uptake is only considered via the venous end. The surface of this geometry is as wide as 70 μm, which is the same size as the surface area of each papilla. The drug uptake was calculated for the periodic model, and at the end, it was scaled up to the actual size of a fentanyl patch. The measurements regarding the geometry sectors are provided in Table 2.

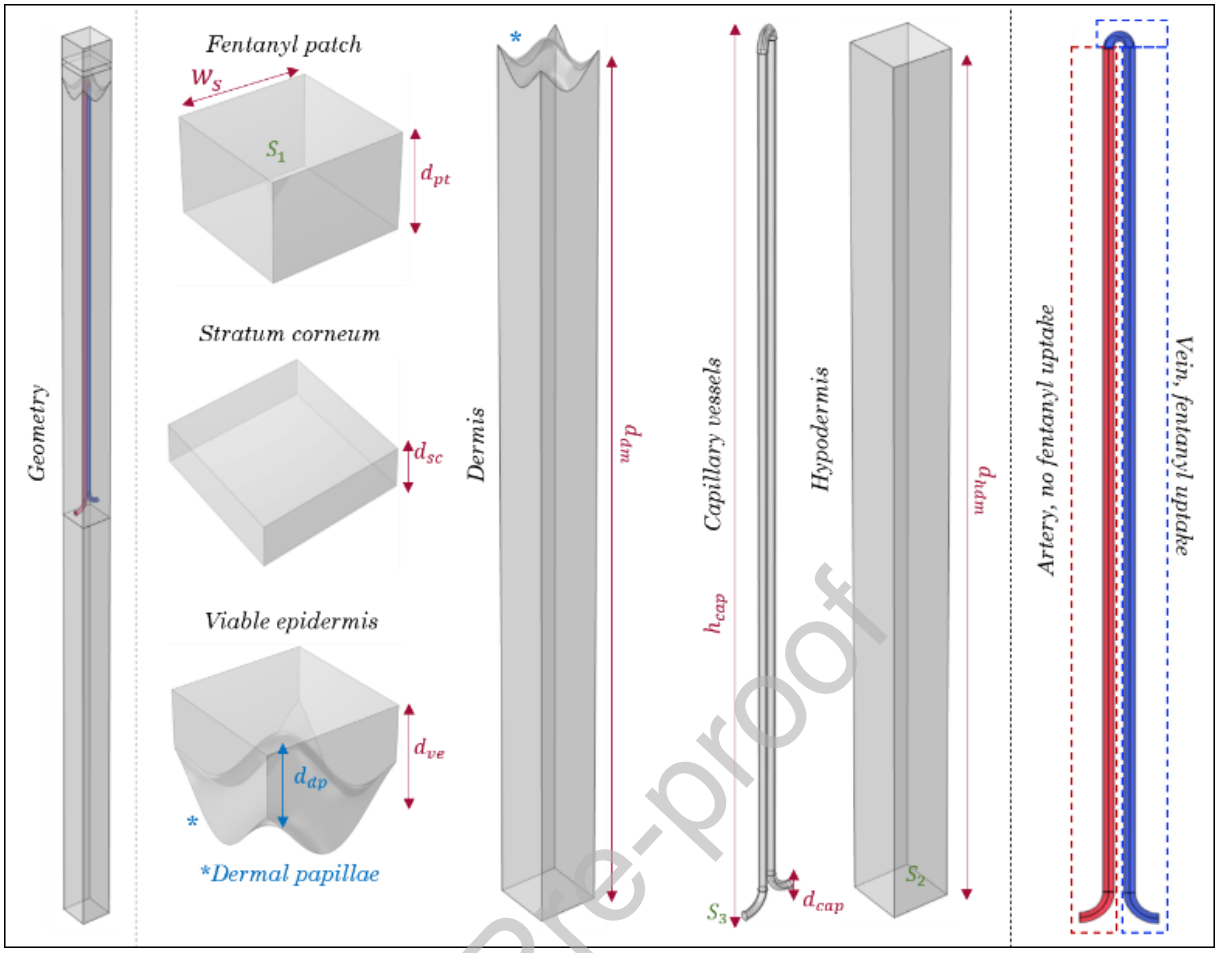

Figure 2- Geometry of fentanyl patch and skin layers included in the drug uptake model (Created by COMSOL Multiphysics software).

2.1.1.2 Blood flow in the capillaries

Due to the small diameter of capillary vessels and low blood flow, the Reynolds number for flow in capillaries is 0.001, corresponding to creeping flow, an extreme case of laminar flow [34]. On the other hand, blood is a non-Newtonian flow, although it shows Newtonian behavior in many cases [35]. However, the presence of red blood cells in the capillaries would reduce the accuracy of blood flow results from the Navier-Stokes model [36]. Nevertheless, for simplification in this study, we assumed that blood in capillaries has a Newtonian behavior, and we implemented Navier-Stokes equation to model it [37].

$$\rho(u_b.\nabla)u_b = \nabla.[-pI + \mu(\nabla u_b + (\nabla u_b)^T)] \quad Equation\ 1$$

Here $\rho\ [kg/m^3]$, $u_b\ [m/s]$, $pI\ [Pa]$, and $\mu\ [Pa.s]$ are blood density, blood velocity, pressure field, and dynamics viscosity, respectively. We assumed, for simplicity, that no plasma leaves and enters the capillary system; therefore, continuity is applicable to blood flow under our assumptions.

$\rho \nabla . u_b = 0$ *Equation 2*

The following boundary conditions were applied for blood flow in the capillaries. The blood flow entered from surface S3 in Figure 2 with an average velocity of 0.065 cm/s based on the average blood flow velocity in the capillaries present in the dermis layer [38]. We assumed that the blood flow in contact with the capillary wall (S4) has a 0 m/s velocity. The resting blood flow rate in the skin depends on several factors, such as temperature, age, humidity, and pressure [39,40]. However, for simplicity, we assumed that the blood flow does not change over time and has thus steady states throughout the simulation.

2.1.1.3 Diffusion process

Fick's second law was implemented to monitor the fentanyl penetration from the patch through the skin layers and its uptake by the capillary network (Equation 3). The details of this model are provided in our previous studies [9,20].

$\frac{\partial c_i}{\partial t} = -\nabla . j_i = \nabla . (D_i \nabla c_i) + u_b . \nabla c_i$ *Equation 3*

Where c_i *[kg/m³]*, j_i *[kg/m².s]*, and D_i *[m²/s]* are fentanyl concentration, fentanyl flux, and diffusion coefficient of fentanyl in domain *i*, respectively. These domains include patch, SC, viable epidermis, demis, capillaries, and hypodermis. However, solving the above equation is computationally demanding due to the different partition coefficients between different layers. Therefore, drug potential instead of drug concentration was used as it is continuous throughout the geometry. Drug potential is connected to drug concentration based on the partition coefficients.

$c_i = \frac{k_i}{k_j} \psi i = K_{i/j} \psi i$ *Equation 4*

Where k_i *[-]* and ψ_i *[kg/m³]* are drug capacity and drug potential in domain *i*, respectively. $K_{i/j}$ *[-]* is the partition coefficient at the interface of domain *i* and *j*.

2.1.2 Pharmacokinetics model

As fentanyl is taken up by the bloodstream, it gets distributed throughout the body, metabolized in the liver, and excreted through the renal system. To track fentanyl's journey in the body, especially its concentration in the plasma, we implemented a lumped Physiological-Based Pharmacokinetic (PBPK) modeling approach [24]. Our model contains five compartments, each representing different organs based on their function. The first compartment is the central compartment, including blood circulation and the lungs (Equation 5). Fentanyl flux from the skin layers enters this compartment (Equation 6). The second compartment is the rapid-equilibrated compartment,

including the heart, brain, skin, and kidneys (Equation 7) [24]. The third compartment is the slow-equilibrated compartment, which consists of muscle, carcass, and adipose tissue (Equation 8) [24]. The fourth compartment represents the gastrointestinal tract, involving the spleen, gut, and pancreas (Equation 5). Lastly, the fifth compartment is the hepatic compartment, where fentanyl metabolism occurs (Equation 6).

$$\frac{\partial c_p}{\partial t} = flux_f \frac{A}{V_c} - \left(k_{cs} + k_{cr} + k_{cl} + k_g - k_{re}\right)\ f_u\, c_p + k_{rc}c_r + k_{sc}c_s + k_{hc}c_l \quad \textit{Equation 5}$$

$$j = -DK_{dermis/cap}\, \Delta c/d_{cap} \quad \textit{Equation 6}$$

$$\frac{\partial c_r}{\partial t} = k_{cr}c_p - k_{rc}c_r \quad \textit{Equation 7}$$

$$\frac{\partial c_s}{\partial t} = k_{cs}c_p - k_{sc}c_s \quad \textit{Equation 8}$$

$$\frac{\partial c_g}{\partial t} = k_{cg}c_p - k_{gl}c_g \quad \textit{Equation 9}$$

$$\frac{\partial c_l}{\partial t} = k_{cl}c_p - k_{lc}c_l + k_{gl}c_g - k_{met}c_l \quad \textit{Equation 10}$$

Where c_i $[kg/m^3]$, k_{ij} $[s^{-1}]$, f_u [%], $flux_f$ $[kg/m^2 s]$, k_{re} $[s^{-1}]$, and k_{met} $[s^{-1}]$ are fentanyl concentration in compartment i, first-order equilibrium rate constant from compartment i to j, unbound fraction of fentanyl, fentanyl flux to the blood circulation, renal clearance constant rate, and metabolism constant rate, respectively. D , $K_{dermis/cap}$, Δc, and d_{cap} are diffusion coefficient of fentanyl in dermis, partition coefficient of fentanyl between dermis and blood, concentration difference between dermis and capillaries, and thickness of capillary's wall, respectively. The general overview of the pharmacokinetics model is shown in Figure 3.

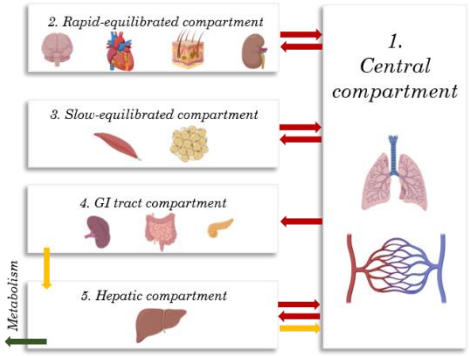

Figure 3- The compartments involved in the pharmacokinetics model. (Created with BioRender.com)

2.1.2.1 Validation of drug uptake model with capillaries using plasma fentanyl concentration

In our previous studies, we validated fentanyl uptake from the patch through the stratum corneum and viable epidermis [20,41] and fentanyl concentration was calculated by the pharmacokinetics model based on fentanyl uptake by skin model [22]. In this study, the skin model includes dermal papillae, dermis layer, capillary network, and hypodermis layer, which are not present in the prior validated drug uptake model. In order to validate the drug uptake model, we compared the evaluated fentanyl concentration in plasma by validated pharmacokinetics model to our previous model, in which the geometry included four blocks as a patch, SC, viable epidermis, and dermis. The thickness of the dermis was only a fraction of the whole dermis and was calculated based on the reported time lag of the fentanyl patch reported in the literature [22]. Additionally, we compared the simulated data with experimental data from the Marier et al. 2006 clinical study [42]. In their study, they had 24 male subjects aged 18 to 45 years old, with a BMI of 18 to 27 kg/m^2 and a minimum weight of 60 kg. In this study, they implemented a fentanyl patch with a nominal flux of 50 μg/h on the upper arm of the volunteers. In order to evaluate the accuracy of the prediction of our model, we calculated the normalized root-mean-square deviation (NRMSD) and area under the curves (AUC). Due to the lack of multiple observations for reported experimental data and simulated data, statistical analysis methods like ANOVA, which require multiple observations, could not be performed. Therefore, the experimental and simulation AUC and Cmax where compared via percentage changes.

2.1.3 Pharmacodynamics model

There is a time lag between the concentration of fentanyl in plasma and the corresponding effect on pain relief. To take into account this time lag, an imaginary compartment, called the effect compartment, is considered. The concentration of fentanyl in the effect compartment by the biophase model is described in Equation 11 to connect the concentration in plasma to the therapeutic effect. [43].

$$\frac{\partial c_e}{\partial t} = k_e \times (c_p - c_e) \quad \textit{Equation 7}$$

Where c_e $[kg/m^3]$, k_e $[s^{-1}]$, and c_p $[kg/m^3]$ are fentanyl concentration in the effect compartment, first-order equilibrium rate constant to the effect compartment, and fentanyl concentration in plasma, respectively. To calculate the pain intensity during fentanyl transdermal therapy, the sigmoid E_{max} model is implemented (Equation 8) [43]. In E_{max} model, the therapeutic effect depends on the maximum response, the concentration related to half of the maximum response, the concentration of the drug in effect

or central compartment, and the hill coefficient. The hill coefficient describes the steepness of the relationship between drug concentration and therapeutic effect [43].

$$E_{pain} = E_{pain}^{0} - E_{pain}^{max} \times \left(\frac{c_e^{\gamma_{pain}}}{EC_{50,pain}^{\gamma_{pain}} + c_e^{\gamma_{pain}}}\right) \quad Equation\ 12$$

Where E_{pain}, E_{pain}^{0}, E_{pain}^{max}, γ_{pain} $[-]$, and $EC_{50,pain}$ $[kg/m^3]$ are pharmacological pain intensity (based on the VAS scale), the initial pain intensity, maximum possible pain relief, Hill coefficient, and concentration of half-maximum effect of fentanyl for pain relief.

2.1.4 Impact of the application site on fentanyl uptake

The skin properties, such as the thickness of skin layers, vary all around the body. Therefore, applying the same fentanyl patch on different body sites will lead to a different outcome. Based on the SmPC (Summary of Product Characteristic) of the Duragesic® fentanyl patch, the fentanyl patch can be applied on the chest, upper arm, back, and flank. The thickness of skin layers in mentioned body sites is detailed in Table 2.

2.1.5 Impact of temperature on fentanyl uptake

The diffusion coefficient of fentanyl in the skin is temperature-dependent. With rising temperatures, the diffusion coefficient of fentanyl exhibits a concurrent increase [44]. Consequently, a fentanyl dosage appropriate for a patient under one thermal condition could potentially result in over- or under-dosage for the patient experiencing a different thermal scenario. To predict this change, we used the well-known Arrhenius equation [32].

$$D_{T_2} = D_{T_1} exp(-E(1/T_1 - 1/T_2)/R) \quad Equation\ 13$$

Where $D_{T_2}[m^2/s]$, D_{T_1} $[m^2/s]$, E $[J/mol]$, and R $[J/mol.K]$ are diffusion coefficient at the temperature T_1, diffusion coefficient at the temperature T_2, the activation energy of diffusion, and the gas constant, respectively. Which here T_1 is considered 33 °C, and D_{T_1} for the patch, SC, the viable epidermis [20], and dermis [45] were chosen based on our previous studies and the literature. Additionally, we assumed the diffusion coefficient of fentanyl in hypodermis is similar to the dermis.

2.1.5.1 Heat transport modeling to calculate temperature distribution throughout the skin

As temperature impacts fentanyl uptake, we aimed to employ the characteristics of fentanyl thermally to enhance the fentanyl uptake by the skin in order to keep the fentanyl concentration in plasma and, eventually, the pain intensity in a desired range.

To this end, we change the temperature at the surface of the fentanyl patch. We implemented the Pennes bioheat transfer equation to monitor the skin's temperature distribution (Equation 14) [46].

$$\rho_i c_{hi} \frac{\partial T}{\partial t} = \kappa_i \nabla^2 T - \omega_b \rho_b c_{hb} (T - T_b) + q_{met} \qquad \textit{Equation 14}$$

Where ρ_i $[kg/m^3]$, c_{hi} $[J/kg.K]$, κ_i $[W/m.K]$, ω_b $[m^3/s.m^3]$, ρ_b $[kg/m^3]$, and c_{hb} $[J/kg.K]$ are the density of skin layer i, the heat capacity of skin layer i, the thermal conductivity of skin layer i, blood perfusion rate, blood density, and the heat capacity of the blood, respectively. T $[K]$, T_b $[K]$, and q_{met} $[W/m^3]$ are temperature, blood temperature, and metabolic heat generation, respectively. Additionally, we considered the temperature at Surface S_2 and S_3 (in Figure 2) to be constant and equal to the average skin temperature.

2.1.5.2 Skin temperature variability through different seasons

The ambient temperature changes considerably during different seasons, which, based on the patient's activity states and clothing, may cause skin temperature and blood flow variations. In this study, we assume no changes happen in the thickness and diameter of the capillaries, and the changes in blood perfusion rate only appear in blood velocity. The changes in skin temperature can lead to changes in the fentanyl diffusion coefficient in skin layers and, eventually, the uptake of fentanyl. Therefore, the same fentanyl patch for one patient in different seasons may lead to different outcomes. In order to study this impact, we considered four scenarios, as listed in Table 1.

Table 1- Summary of four scenarios considered for the impact of seasonal change in skin temperature and blood perfusion rate

Scenario	Season	Room temperature	Clothing	Activity level	Body sites	Outputs
1	Winter	18.0 – 20.5 [℃] Ref. [47]	Sweatpants, a light jumper, socks During reclining in bed: covering with a duvet	Remained in a supine position	Chest Back Flank Upper arm	Skin temperature and blood perfusion rate
2	Winter			Limited to reclining in bed for sleep, remaining indoors, and minimum daily activity		
3	Summer	27.8 – 34.3 [℃] Ref. [48]	T-shirt, shorts, no socks During reclining in bed: covering with a blanket	Remained in a supine position		
4	Summer			Limited to reclining in bed for sleep, remaining indoors, and minimum daily activity		

The human thermoregulation model predicting human thermal response in an awake state to the environmental conditions at a given activity level and clothing situation [49,50] was used to simulate corresponding skin temperatures and blood perfusion rates at body location of interest. The model is based on the bioheat equation describing the energy balance of the human body and regression equations modulating skin blood perfusion rates, sweating, and shivering thermogenesis. The validity of the model was proven in several validation studies, including mean skin and core temperatures as well as local skin temperatures [51–53]. Clothing was addressed using data from a thermal manikin study [54] to account for possibly the most realistic conditions of the thermal exposure.

The variation in skin temperature at different anatomical sites during the scenarios outlined in Table 1 is illustrated in Figure 4. As shown in Figure 4a&b, the skin temperature on the chest varies in summer from 33.9 °C to 35.2 °C for the inactive state, and for the active state, it varies between 33.8-35.4 °C. However, in winter, there is an almost 3 °C difference between the average skin temperature of the flank, chest, and back. Furthermore, as shown in Figure 4c&d, the skin temperature on the chest during winter for the inactive state varies from 31.9 °C to 33.8 °C and for the active state, from 32.4 °C to 34.0 °C. As skin temperature varies, so does the blood perfusion rate, as depicted in Figure 4e. Based on this result, the blood flow rate changes from 304% (vasodilation) of the thermoneutral state to 13.2% (vasoconstriction) when transitioning from the active state in summer to the inactive state in winter.

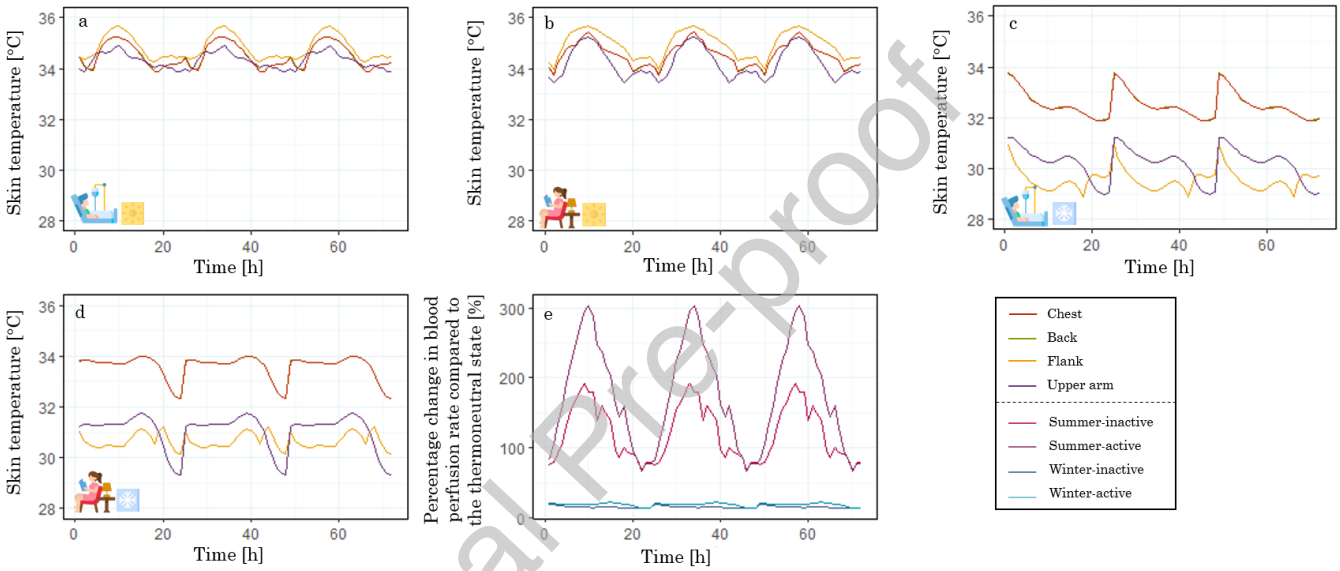

Figure 4- Skin temperature of the chest, back, flank, and upper arm during a: inactive state in summer, b: active state in summer, c: inactive state in winter, and d: active state in winter; e: the percentage blood flow rate compared to the base state during active and inactive states in summer and winter. (Created with elements from www.flaticon.com)

2.1.5.3 Thermally-controlled fentanyl transdermal delivery

The diffusion coefficient of fentanyl in skin layers depends on the temperature. As the temperature increases, the diffusion coefficient of fentanyl; subsequently, the fentanyl flux from the skin and, eventually, the fentanyl concentration in plasma increases. In this study, we aimed to use this behavior of fentanyl in response to heat to steer the fentanyl transdermal therapy in order to keep the fentanyl concentration in plasma and its corresponding effects in a favorable range. To reach this end, we used the event interface of COMSOL Multiphysics to control the state of applying heat to the fentanyl patch to increase the temperature of the outer surface of the fentanyl patch to a maximum of 43.5 °C. Our goal was to maintain the fentanyl concentration below 2 ng/ml, pain intensity (VAS) below 3, and the stratum corneum temperature below 43 °C. However, in all cases, the fentanyl concentration remained below the 2 ng/ml limit, making this criterion unnecessary. The threshold of 43 °C for the temperature of SC was chosen since 43 °C is the highest temperature the skin can tolerate for a long time without disturbing the blood flow [55]. Additionally, a higher temperature, like 44 °C, is the threshold of skin temperature for pain sensation [56], and tissue injury will occur if the skin stays at this temperature for at least six hours [57]. When the applying heat is off, we assumed the temperature of the outer surface of the patch switches back to 33 °C, which is a normal skin surface temperature [58]. Therefore, the conditions below were applied.

$$\begin{cases} pain > 3 \ \ and \ T_{sc} \leq 43\ [℃] \rightarrow heat\ on \\ pain \leq 3 \ or \ \ T_{sc} > 43\ [℃] \rightarrow heat\ off \end{cases}$$

2.1.5.4 Validation of temperature impact on fentanyl concentration in plasma

To assess the digital twin's predictive accuracy in understanding heat's impact on fentanyl uptake, we compared the calculated values by digital twin with the measured values in the study done by Shomaker et al. [59]. Their study involved six healthy volunteers aged 18 to 50, weighing 55 to 100 kg. Fentanyl patches with a nominal flux of 25 μm/h were applied on the upper right anterior chest, with experiments conducted both without heat and with 4 hours of heat application until the skin reached 41℃. In the Shomaker et al. study, the heat flux, the baseline skin temperature without heat, and changes in the temperature profile of the skin are not provided. Therefore, we assumed the skin temperature during no-heat duration to be the average skin temperature of the chest (34.2 ℃ [60]) and 41 ℃ while applying the heat. To evaluate the prediction performance of the digital twin in the impact of heat on drug uptake, NRMSD was calculated.

2.2 Estimation of model parameters

The value of implemented parameters used in blood flow, drug uptake, pharmacokinetics, pharmacodynamics, and temperature distribution model used in this study is provided in Table 2. The parameters implemented in the drug uptake model, pharmacokinetics model, and pharmacodynamics were validated in our previous studies [20,22].

Table 2- Parameters implemented in the developed digital twin

Model	Parameter	Description	Value/Equation	Ref.
Geometry	d_{sc}	*Thickness of the stratum corneum*	$chest$: 19.7 , $back$: 15.4 , $flank$: 12.8, $upperarm$: 15.3[μm]	61,62
	d_{ve}	*Thickness of the viable epidermis*	$chest$: 78.8 , $back$: 61.4 , $flank$: 51.08, $upperarm$: 61.1[μm]	61,62
	d_{de}	*Thickness of the dermis*	$chest$: 1400 , $back$: 1941 , $flank$: 1070.9, $upperarm$: 987[μm]	61,62
	d_{hd}	*Thickness of the hypodermis*	1000[μm]	-
	d_{pt}	*Thickness of the patch*	50.08[μm]	63
	d_{dp}	*Hight of dermal papillae*	34[μm]	64
	h_{cap}	*Height of capillary vessel*	$d_{de} - 22$ [μm]	-
	d_{cap}	*Diameter of capillary vessel*	10 [μm]	65
	d_c	*Diameter of the capillary curve*	23 [μm]	-
	w_s	*Width of the block*	46.6 [μm]	66
Blood flow	p_b	*Pressure in the capillary vessel*	30 [$mmHg$]	67
	ρ_b	*Density of blood*	1060 [kg/m^3]	46
	μ_b	*Dynamic viscosity of blood*	$4.5 * 10^{-3}$ [$Pa.s$]	68
	U_{in}	*Average velocity of inlet blood flow*	0.065 [m/s]	38
Drug uptake	D_{pt}	*Diffusion coefficient of patch*	$7.03 * 10^{-16} * \exp(E * (T\_pt\ [K] - 306.15[K])/(R * T\_pt\ [K] * 306.15[K]))$	20,32
	D_{sc}	*Diffusion coefficient of SC*	$3.0 * 10^{-14} * \exp(E * (T_{sc}[K] - 306.15[K])/(R * T_{sc}[K] * 306.15[K]))$	20,32
	D_{ve}	*Diffusion coefficient of the viable epidermis*	$3.0 * 10^{-14} * \exp(E * (T_{ve}[K] - 306.15[K])/(R * T_{ve}[K] * 306.15[K]))$	20,32

	D_{de}	*Diffusion coefficient of dermis*	$3.61 * 10^{-11} * \exp(E * (T_{de}[K] - 306.15[K])/(R * T_{de}[K] * 306.15[K]))$	[22,32]
	D_{hd} *	*Diffusion coefficient of hypodermis*	$3.61 * 10^{-11} * \exp(E * (T_{hd}[K] - 306.15[K])/(R * T_{hd}[K] * 306.15[K]))$	-
	D_{cap}	*Diffusion coefficient of capillary*	$3.0 * 10^{-13} * T_{cap}$	Stokes–Einstein equation
	$K_{pt/sc}$	*Partition coefficient between patch and sc*	$\frac{1}{3.4}$	[20]
	$K_{sc/ve}$	*Partition coefficient between sc and viable epidermis*	1	[20]
	$K_{ve/de}$	*Partition coefficient between viable epidermis and dermis*	1	-
	$K_{de/hd}$	*Partition coefficient between dermis and hypodermis*	1	-
	$K_{de/cap}$	*Partition coefficient between dermis and blood*	1.84	[24]
Pharmacokinetics model	V_c	*Volume of the central compartment*	26.4 $[L]$	[24]
	V_r	*Volume of the rapid-equilibrated compartment*	27.1 $[L]$	[24]
	V_s	*Volume of the slow-equilibrated compartment*	894.6 $[L]$	[24]
	V_g	*Volume of GI-tract compartment*	19.2 $[L]$	[24]
	V_h	*Volume of the hepatic compartment*	22.6 $[L]$	[24]

$Q_{c/r}$	*Blood flow from central to rapid-equilibrated compartment*	1.58 $[L/min]$	[69]
$Q_{c/s}$	*Blood flow from central to slow-equilibrated compartment*	2.04 $[L/min]$	[69]
$Q_{c/g}$	*Blood flow from central to GI-tract compartment*	0.68 $[L/min]$	[69]
$Q_{c/l}$	*Blood flow from the central to hepatic compartment*	0.162 $[L/min]$	[69]
k_{cr}	*First-order equilibrium rate constant from central to rapid-equilibrated compartment*	$Q_{c/r}/V_c$	-
k_{rc}	*First-order equilibrium rate constant from rapid-equilibrated to the central compartment*	$Q_{c/r}/V_r$	-
k_{cs}	*First-order equilibrium rate constant from central to slow-equilibrated compartment*	$Q_{c/s}/V_c$	-
k_{sc}	*First-order equilibrium rate constant from slow-equilibrated to the central compartment*	$Q_{c/s}/V_s$	-

	k_{cg}	*First-order equilibrium rate constant from central to GI-tract compartment*	$Q_{c/g}/V_c$	-
	k_{gl}	*First-order equilibrium rate constant from GI-tract to hepatic compartment*	$Q_{c/g}/V_g$	-
	k_{cl}	*First-order equilibrium rate constant from central to hepatic compartment*	$Q_{c/l}/V_c$	-
	k_{lc}	*First-order equilibrium rate constant from hepatic to the central compartment*	$Q_{c/l}/V_l$	-
	f_u	*Fraction of unbound fentanyl*	0.21	[70]
	k_{re}	*First-order equilibrium rate constant for renal clearance*	0.000026 $[s^{-1}]$	[71]
	k_{met}*	*First-order equilibrium rate constant for metabolism*	0.002 $[s^{-1}]$	[71]
Pharmacodynamics model	$k_{e,pain}$	*first-order equilibrium rate constant of fentanyl for the pain relief effect*	0.31 $[min^{-1}]$	[71]
	γ_{pain}	*Hill coefficient for pain relief*	2.7	[22]
	$IC_{50,pain}$	*Concentration of half-maximum effect of fentanyl for pain relief*	1.27 $[ng/ml]$	[22]
Heat	T_{skin}	*The skin temprature*	$chest$: 34.2 , $back$: 34.8 , $flank$: 35.0, $upperarm$: 33.1[℃]	[60]

E	*Activation energy of diffusion*	61 $[kJ/mol]$	11
R	*Gas constant*	8.314 $[j/(mol.K)]$	-
c_{hi}	*Heat capacity*	$patch^{**}$: 1930 , SC & $viable\ epidermis$: 3589 , $dermis$: 3300, $hypodermis$: $[j/(kg.K)]$	72,73
c_{hb}	*Heat capacity of the blood*	3210 $[j/(kg.K)]$	46
ρ_i	*Density*	$patch^{**}$: 1090 , $skin$: 1200 $[kg/m\text{^}3]$	72,74
ω_b	*Blood perfusion rate (blood volume per second through the tissue volume)*	0.02 $[m^3/(s.m^3)]$	72,75
κ^*	*Thermal conductivity*	$patch^{**}$: 0.38, SC & $viable\ epidermis$: 0.235, $dermis$: 0.445, $hypodermis$: 0 $capillaries$: 0.467 $[W/(m.K)]$	76–78
q_{met}	*Metabolic heat generation*	368.1$[W/m\text{^}3]$	46

**** We assumed that the diffusion coefficient of fentanyl in the hypodermis layer is the same as the dermis layer***

***** Due to a lack of sufficient information on the thermal properties of the fentanyl patch, the reported values are for polyester, one of the present materials in the fentanyl transdermal patch based on the Duragesic label*** [79]

2.3 Spatial and temporal discretization

Tetrahedral elements were employed to grid the skin layers and capillary networks, with the number and distribution of these grids selected based on the involved physics. Notably, the density of these grids increased at the interfaces. Due to variations in thickness at different body sites, the number of grids differed accordingly. For evaluating the blood velocity in the capillary network in the fluid flow model, the number of grids ranged from 47,503 to 55,837. In contrast, the number of grids for calculating the fentanyl flux through the skin layers varied between 1,811,291 and 3,184,822. This variation in the number of grids for each model was due to the changes in skin layer thickness on different anatomical sites. The simulations were conducted for a maximum of 72 hours (3 days), matching the application time of the fentanyl transdermal patches. The COMSOL model determines the time steps implicitly based on the BDF (Backward differentiation formula) method; however, for achieving high temporal resolution in the recorded data, we chose a time step of 0.1 h.

2.4 Numerical implementation and simulation

COMSOL Multiphysics version 6.1 was utilized to simulate various aspects, including blood flow in the capillaries, fentanyl penetration through the skin, fentanyl distribution and elimination in the body, fentanyl effects, and temperature distribution in skin layers. The solver scheme employed in this study was MUMPS (MUltifrontal Massively Parallel sparse direct Solver). A laminar flow module and stationary study were used for blood flow in the capillary network. Fentanyl penetration through the skin and temperature distribution in skin layers were modeled through partial differential equations (PDEs) and time-dependent studies. The pharmacokinetics model was established using boundary ordinary differential equations (ODEs) and time-dependent studies. The concentration of fentanyl in the effect compartment was calculated using the ODE interface, and the effects of the drug were analyzed using boundary probes and time-dependent studies. The event interface and time-dependent study were employed to control the heating state.

3 Results and discussion

3.1 Fentanyl uptake by the skin

3.1.1 Validation of drug uptake model with capillaries using plasma fentanyl concentration

Implementing the information from Section **Error! Reference source not found.** on the subjects and the condition outlined in the Marier et al. 2006 study [42], we calculated the

fentanyl concentration in plasma using our study's developed digital twin. Based on the result shown in Figure 5, our previous study's NRMSD (normalized root-mean-square deviation) is 0.15, and the current model is 0.1. Therefore, the current model predicted closer values to experimental data. The time to reach the maximum concentration (t_{max}) for the current model is 36 h, which is the same as the experimental data; however, for our previous model, it is 23 h (only based on the recorded times, not the actual one). The maximum fentanyl concentration in plasma for experimental data is 1.7 ng/ml; for the previous model, it is 1.2 ng/ml (3% lower), and for the current model, it is 1.1 ng/ml (11% lower). The area under the curve for experimental data is 64.7 ng h/ml; for the previous model is 69.4 ng h/ml (7.7% more), and for the current model is 63.7 ng h/ml (1.5% less). To conclude, this new model with blood flow not only predicts the fentanyl concentration in the plasma closer to the experimental data and with a similar area under the curve but also predicts the t_{max} more accurately. However, compared to our previous model, the predicted maximum concentration of fentanyl in the plasma is 8% less than in experimental data. In this Figure, error bars are not included as they are not reported in the original study. This should be taken into account when interpreting the comparison between the experimental and simulation data.

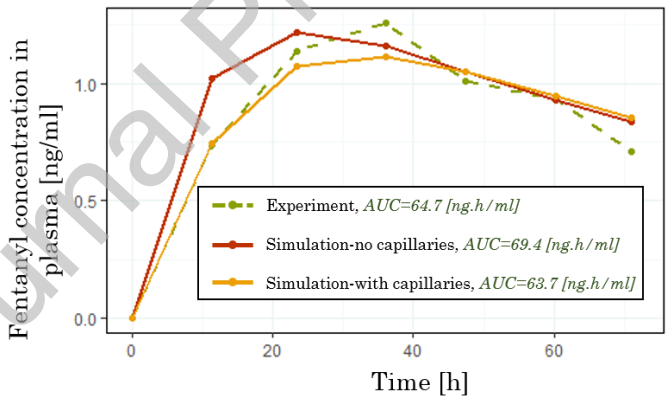

Figure 5- Fentanyl concentration in the plasma during 72 hours of applying one fentanyl patch with a nominal flux of 50 [µg/h]. (The green curve is obtained from a clinical study by Marier et al. 2006 [42], and the red curve is based on results from the Bahrami et al. study [22]).

3.2 Impact of application site on fentanyl uptake

We virtually applied a fentanyl patch with a nominal flux of 50 $\mu m/h$ on the chest, back, flank, and upper arm of a virtual patient with a body mass of 70 kg and age of 60 years old. These locations vary from each other based on their skin layers' thickness and skin temperature, which values are provided in Table 2. Based on the results in Figure 6a, the main deviation in fentanyl flux from the path to different body sites

occurs at the initial time. The main cause of this variation is the different skin temperatures, which lead to different diffusion coefficients. The fentanyl flux toward the capillary networks is shown in Figure 6b. Based on this result, the flux of fentanyl in different application sites is considerably different from each other; however, except for the patch on the flank, the fentanyl concentrations in plasma (Figure 6c) are very similar. The reason is that besides the flux, the capillary surface area that the fentanyl penetrates through differs in each of them, which is directly dependent on dermis thickness. For example, the fentanyl flux for the upper arm is higher compared to the back, which is 93% more, while the dermis thickness is 49% less. Therefore, the capillary surface area for fentanyl uptake in the upper arm is considerably less than in the back. Additionally, the maximum concentration of fentanyl in plasma (c_{max}) and time to reach this maxmimum concentration (t_{max}), the most two important pharmacokinetics parameters vary for different application sites. The t_{max} when fentanyl patch is applied on the upper arm happens 10.3 h later than the flank, on the other hand, the c_{max} when the fentanyl patch is applied on the flank is 15.3% higher than the chest. Howevere, the difference in c_{max} when the patch is applied on the upper arm and the back is only 1.2% and 1.7% higher than the chest. As expected, the calculated pain intensity only when the patch is applied on the flank is considerably different from the other application sites. However, for none of the applications, the pain intensity reaches VAS 3, which is a medium pain intensity and the target outcome in this study. From these findings, applying the same fentanyl patch for the same patient on different anatomical sites can lead to different outcomes. Consequently, the effectiveness of a fentanyl patch in managing the pain on one anatomical site does not guarantee success on another site.

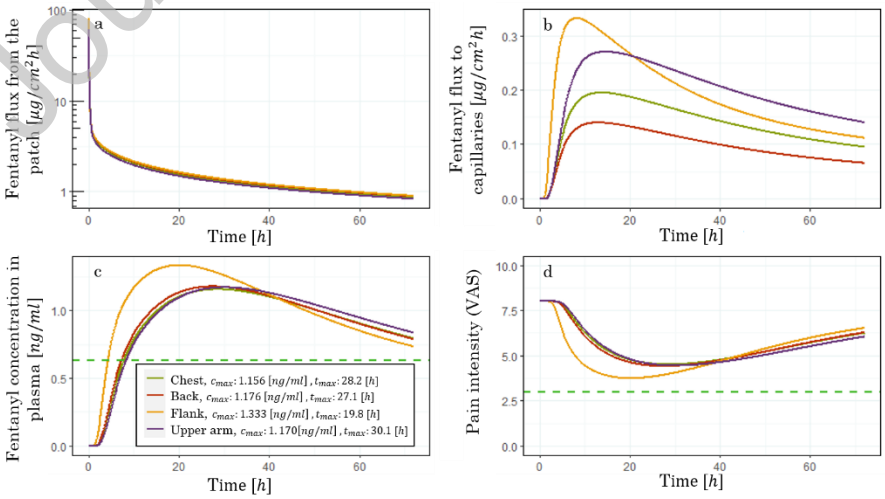

Figure 6- the impact of the application site, including chest, back, flank, and upper arm on a: fentanyl flux from the patch; b: drug uptake flux by capillaries; c: fentanyl concentration in plasma; and d: pain intensity

3.3 Thermal impact on fentanyl transdermal therapy

3.3.1 Validation of temperature impact on fentanyl concentration in plasma

Based on the conditions and information on the subjects of the experiment in the Shomaker et al. study [59] provided in Section 2.1.5.4, we calculated the fentanyl concentration in plasma with and without applying heat on the skin and the patch by using the developed digital twin. Figure 7a reveals that the digital twin accurately predicted fentanyl plasma concentration during the no-heat experiment, with an NRMSD of 0.12 and only an 8.4% lower area under the curve compared to the experiment. In the experiment with applied heat (Figure 7b), the NRMSD was 0.15, and the area under the curve for simulated data differed by only 1% from the experiment. However, the maximum heat-induced concentration was 22.7% lower than the experimental data for the simulated data. Focusing solely on the digital twin's prediction of heat effects, the concentration difference between heated and non-heated experiments was examined for both experiment and simulation (Figure 7c). In this figure, The error bars included in the experimental data graphs are estimated as 20% of the mean values, based on the information from the Shomaker et al. 2000 study that the relative standard error and standard deviation were up to 20%. This estimation is conservative, and the actual variability could be less. However, the close alignment of the simulation data with the experimental data, within the range of the error bars, suggests that the simulation model is reasonably accurate. In conclusion, the model could predict the impact of heat on fentanyl concentration in the plasma with a favorable level of agreement, which led to an NRMSD of 0.15.

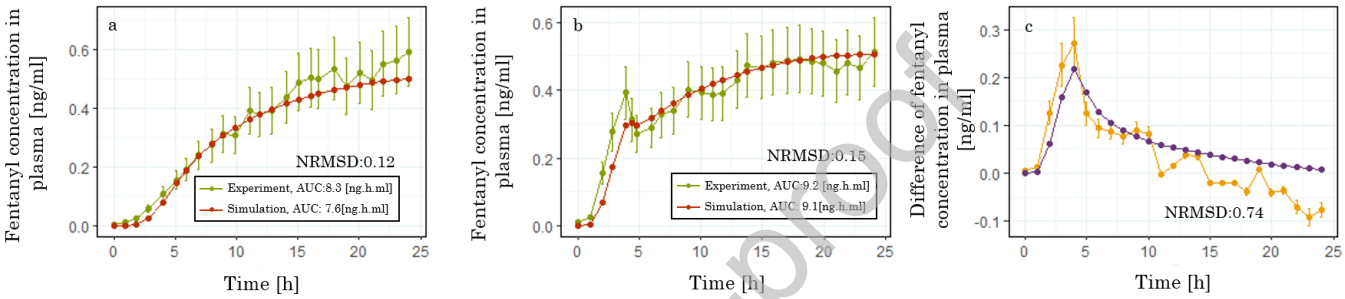

Figure 7- Validation of prediction of digital twin on the impact of heat on fentanyl concentration in plasma (The experimental data is from Shomaker et al. 2000 clinical study). The experimental data points are shown with error bars estimated at 20% of the mean values, based on the original study's report that the relative standard error and standard deviation were up to 20%. This estimation serves as a visual guide for variability. Due to the lack of a precise report of the error bar, the actual error bar in the original study may differ.

3.4 Seasonal impact on fentanyl transdermal delivery

The ambient temperature and skin temperature fluctuate with the changing seasons, transitioning from winter to summer. Moreover, the patient's condition, shifting from inactive to active, will impact skin temperature. Notably, changes in ambient temperature and activity state not only influence skin temperature but also affect the blood perfusion rate within the skin, as demonstrated in Figure 4, based on the conditions provided in Table 1. The results of implementing the calculated skin temperature and blood perfusion rate percentage into the digital twin for the fentanyl patch, with a nominal flux of 50 $\mu g\ h^{-1}$ on the chest, back, flank, and upper arm, are shown in Figure 8. Based on this result, the maximum flux of fentanyl from the dermis layer to the capillaries increases by 1.8%, 2.6%, 11.8%, and 10.3% when transitioning from an inactive state in winter to active states in summer, with the patch applied on the chest, back, flank, and upper arm, respectively (Figure 8a,d,g,&j). Consequently, the maximum fentanyl concentration under the same conditions increases by 0.8%, 0.8, 1.5%, and 4.3% when the patch is applied on the chest, back, flank, and upper arm, respectively (Figure 8b,e,h,&k). As a result of variations in the concentration of fentanyl in the plasma, the minimum pain intensity under the same conditions increased by 0.9%, 1.1%, 2.1%, and 4.9% when the patch is applied on the chest, back, flank, and upper arm, respectively (Figure 8c,f,i,&l). Based on these results, the standard deviation for minimum pain intensity during these scenarios is five times more when the patch is applied on the upper arm than on the chest. This implies the higher impact of ambient temperature and activity when the patch is applied on the upper arm compared to the chest. Therefore, based on the condition described in Table 1, when the average room temperature drops from 31 °C to 19 °C, and the condition of the patient changes from active to inactive, the pain relief can be reduced by up to 4.9%. In cases of more extreme environmental variations, the impact on the outcomes of transdermal fentanyl therapy can be even more substantial. The total amount of released fentanyl in 72h for a fentanyl patch with a nominal flux of 50 μg/h during the mentioned thermal scenarios in Table 1 is shown in Figure 9. Based on these results, the total intake of fentanyl varies between different scenarios, such as the total amount of released fentanyl when the patch is applied on the upper arm during the active state in summer is 8.7% more than the inactive state in winter.

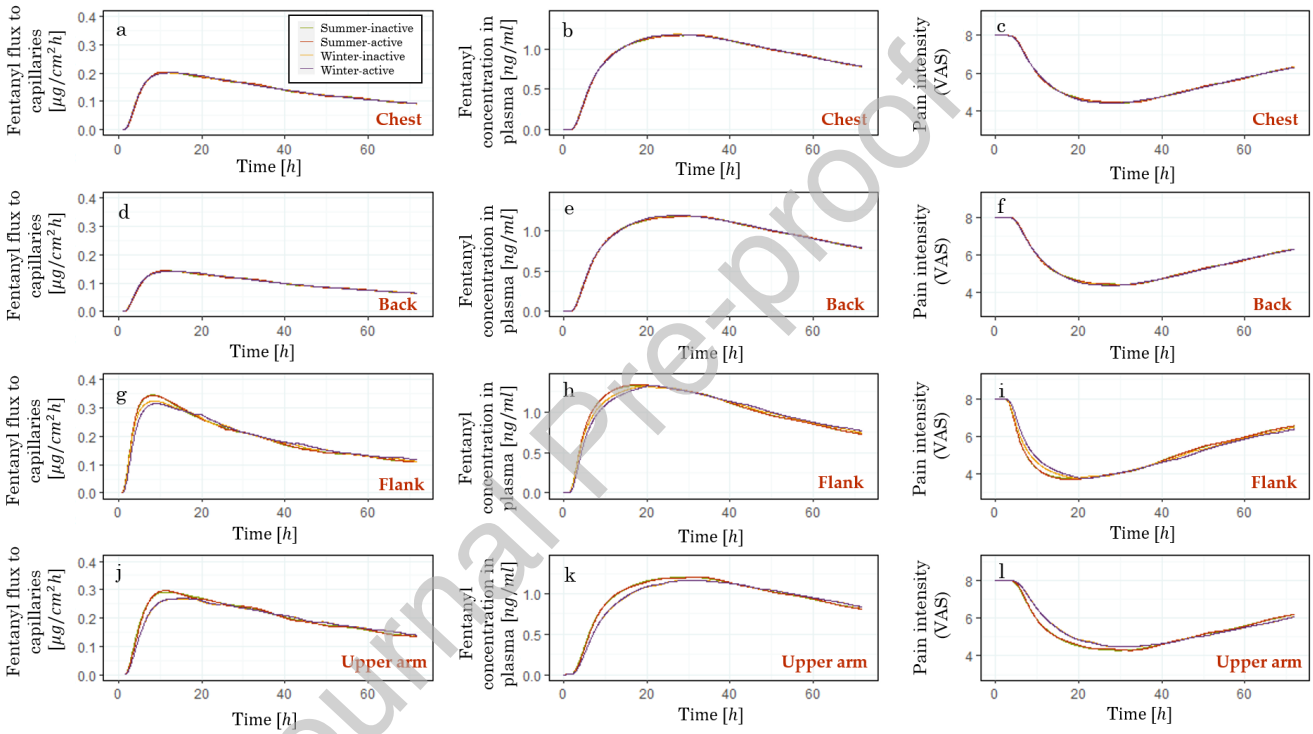

Figure 8- The impact of seasonal change and the activity of the patient on fentanyl flux to capillary (from a: chest, d: back, g: flank, and j: upper arm), fentanyl concentration in plasma (when the patch is applied on the b: chest, e: back, h: flank, k: upper arm), and pain intensity (when the patch is applied on the c: chest, f: back, i: flank, and l: upper arm)

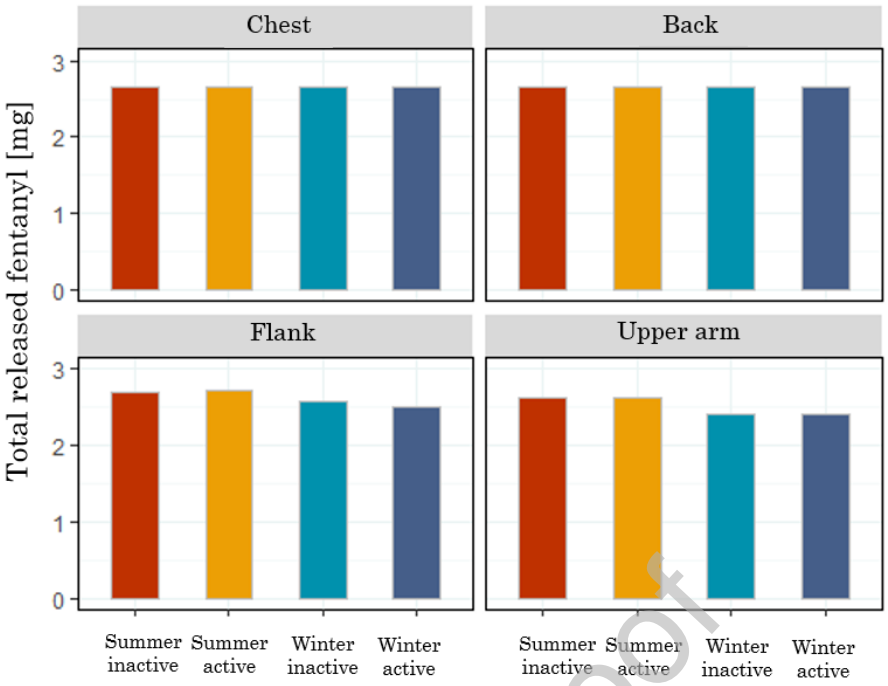

Figure 9- The total amount of released fentanyl from the patch with a nominal flux of 50 $\mu g/h$ during different seasons and activity states.

3.5 Thermally enhanced fentanyl transdermal delivery

3.5.1 Heat distribution in skin layers

The temperature distribution in skin layers and the patch is calculated based on the model provided in Section 2.1.5.1. In order to evaluate the impact of higher temperatures on the outer surface of the fentanyl patch on the diffusion coefficient of fentanyl in skin layers, we explored a range of temperatures from 33 ℃, a normal skin temperature, to 43 ℃, a safe, high temperature for the skin. Here we assumed the temperature at the bottome of hypodermis stay constant and equal to 33℃. As shown in Figure 10/a, by increasing the temperature at the outer surface of the fentanyl patch, the overall temperatures of the patch and skin layers increases; however, the changes decrease as the distance to the patch increases. As the patch surface temperature increases from 33 to 43 ℃, the average temperature of SC changes from 33 to 42.5 ℃, while the average temperature of hypodermis only changes from 33 to 33.3 ℃. Following this, the diffusion coefficients of the patch, stratum corneum, viable epidermis, dermis, hypodermis, and capillary increase by factors of 2.1, 2.1, 2.0, 1.4, 1.0, and 1.0, respectively, when the outer surface of the patch is at a temperature of 43 ℃, in comparison to when it is at 33 ℃. Based on this result, by increasing the outer temperature of the fentanyl patch by 10 ℃, the diffusion coefficient of fentanyl increases considerably, which may lead to higher penetration of fentanyl through the skin and eventually higher fentanyl concentration in plasma.

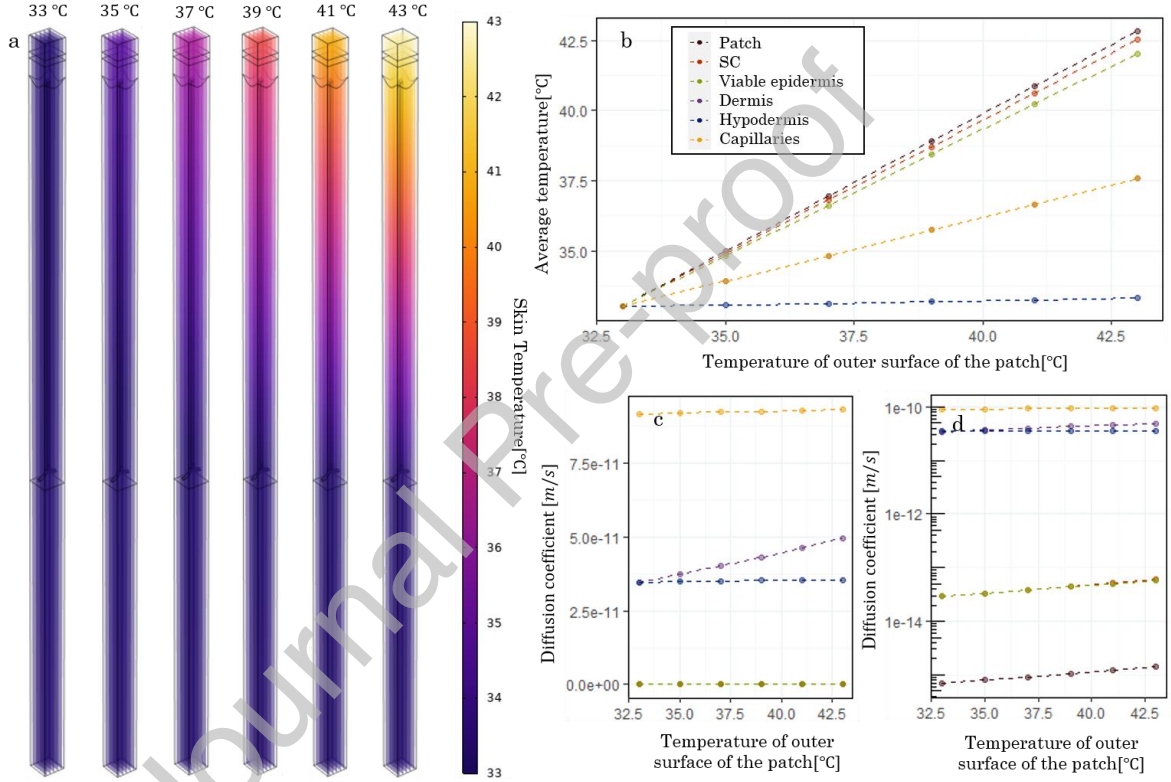

Figure 10- Temperature distribution in the skin and the patch during the application of different temperatures on the outer surface of the patch

3.5.1.1 Thermally-controlled transdermal fentanyl delivery

Based on the results in Section 3.5.1, we aimed to enhance the fentanyl delivery by applying heat on the outer surface of the fentanyl patch. This could be, for example, done by designing a temperature-controlled wearable device or a heating garment and placing it on the patch. The heat application criteria are based on the conditions provided in Section 2.1.5.3. In Figure 11/a,b,&c, the fentanyl concentration in the plasma, pain intensity, and the average temperature of the stratum corneum are shown during 72 hours of fentanyl transdermal therapy with the nominal flux of $50[\mu g/h]$. Based on this result, the virtual patient does not experience pain intensity below three throughout the therapy. However, after applying the heat on the surface of the fentanyl patch, the fentanyl concentration, as a result of the increase in the diffusion coefficient, increases (Figure 11/e). Due to the increase in the fentanyl concentration in plasma, the pain intensity for all the application sites drops below 3. Additionally, as shown in Figure 11f, the average temperature of the stratum corneum was kept under 43 [°C], and the heater's temperature is shown in Figure 11g. The summary of thermally enhanced fentanyl delivery is brought in Table 3.

Based on these results, which implemented controlled higher temperature, the digital twin is able to not only decrease the average pain intensity (between 0.8 to 1.3 units) and increase the time without pain but also reduce the deviation in fentanyl concentration and pain intensity between different application sites. Therefore, the digital twin was able to improve the outcome treatment while reducing the variability between different application sites by implementing higher temperatures on the fentanyl patch.

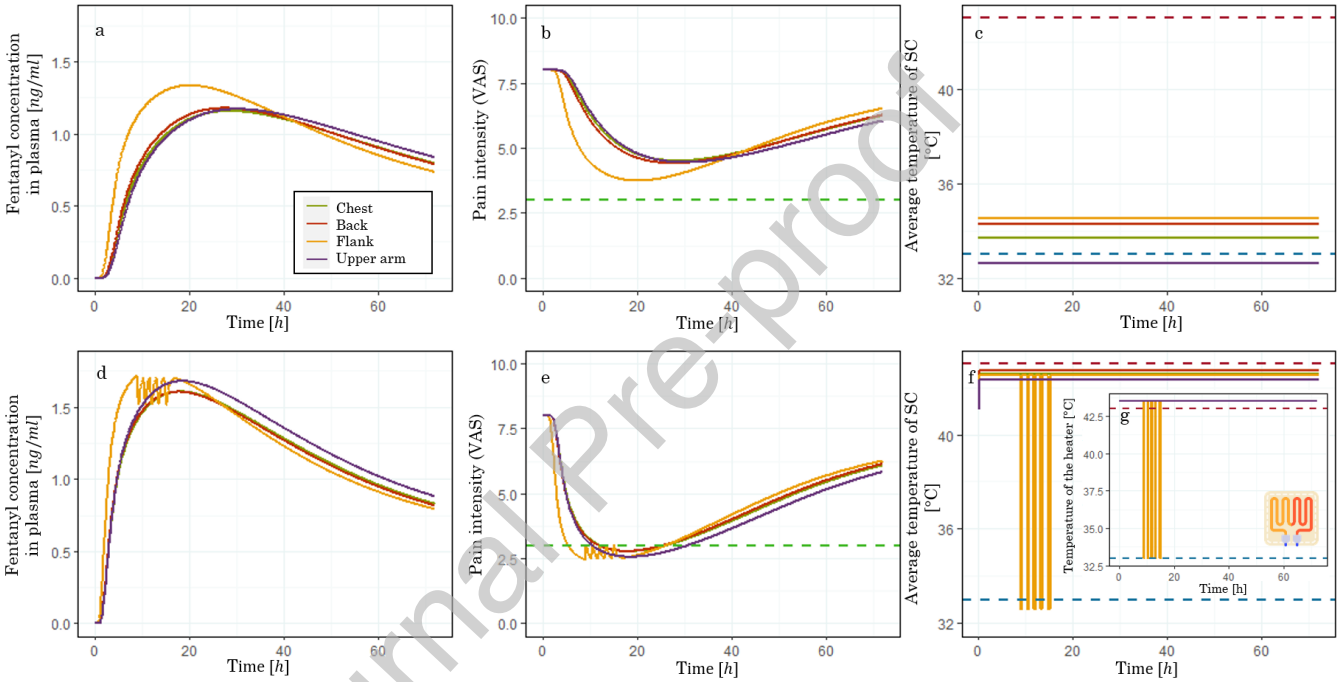

Figure 11- a: Fentanyl concentration in plasma; b: Pain intensity; c: Average temperature of stratum corneum during 72 hours of fentanyl transdermally therapy with applying no heat; d: Fentanyl concentration in plasma; e: Pain intensity; f: Average temperature of stratum corneum during 72 hours of fentanyl transdermally therapy with applying heat on the surface of fentanyl patch with a nominal flux of 50 µg/h. (The heathing icon is created with elements from www.flaticon.com)

Table 3- Summary of the outcome of fentanyl treatment with and without applying heat on the outer surface of the fentanyl patch

	No heat			With heat		
Location	$c_{max}\,[ng/ml]$	Average pain intensity (VAS)	Time without pain [h]*	$c_{max}\,[ng/ml]$	Average pain intensity (VAS)	Time without pain [h]*
Chest	1.16	5.5	0	1.60	4.4	14.6
Back	1.18	5.7	0	1.60	4.4	14.5
Flank	1.33	5.1	0	1.70	4.3	21
Upper arm	1.17	5.4	0	1.68	4.1	20.7
SD	0.08	0.18	-	0.05	0.12	3.6

*** The duration during which the pain intensity is below 3**

4 Outlook

Within the context of this research, we exclusively examined a virtual heater, which affects the temperature of the outer layer of the transdermal fentanyl patch. However, implementing an actual heater onto a transdermal patch would offer valuable insights into its flexibility in temperature adjustments and its limitations. This heater could be linked to a digital twin in order to control its activation and deactivation precisely, therefore providing a safe yet effective control release of fentanyl or other therapeutic substances.

In this study, the developed digital twin of the human body was implemented to monitor and steer transdermal fentanyl penetration through the skin, its distribution and concentration throughout the body, and finally, its therapeutic effect, pain relief. Nevertheless, fentanyl transdermal therapy is one of many examples of transdermal drug delivery systems that can be monitored and adjusted with the help of a physics-based digital twin. A similar approach by including the drug uptake model, pharmacokinetics model, and pharmacodynamics models can be implemented for other therapeutics drugs. Among suitable drugs for transdermal therapy, we can mention Estradiol for menopausal symptoms, Nicotine for smoking cessation, Lidocaine for post-herpetic neuralgia pain, Rotigotine for Parkinson's disease, and Rivastigmine for dementia [80]. Other types of transdermal patches with different drug uptake enhancers can also be investigated. Examples of these patches are iontophoresis, concavitational and cavitational ultrasound, electroporation, and microneedles.

In this study, a new skin model was introduced, which included capillaries with blood flow. This *in-silico* skin model included stratum corneum, viable epidermis, dermal papillae, dermis layer, hypodermis, and capillary network. We used this model to predict fentanyl penetration through the skin layers to reach the blood circulation system. Importantly, this virtual skin model can serve a broader purpose, extending to the assessment of the safety of cosmetics, toiletries, and topical products. This in-silico skin model, integrated with relevant kinetics throughout the body, offers essential insights that are beyond the capabilities of *in-vitro* studies without subjecting animals to the risks inherent in *in-vivo* tests. Therefore, this in-silico skin model holds promise as a valuable tool for physicians.

5 Conclusions

In this study, we developed a physics-based digital twin that includes drug uptake, pharmacokinetics, and pharmacodynamics models of fentanyl transdermal therapy. In this digital twin, an in-silico skin model incorporates stratum corneum, viable epidermis, dermal papillae, dermis, hypodermis, and capillary network. In order to validate the fentanyl uptake from this in-silico model, we compared the calculated fentanyl concentration with our previous model [22] and experimental data from the Marier et al. study [42]. The result showed that the novel skin model successfully predicted the fentanyl concentration in plasma (with NRMSD of 0.1), the area under the curve, and the time to reach the maximum concentration of fentanyl in plasma. However, it evaluated a lower maximum concentration of fentanyl in plasma compared to experimental data and the previous skin model.

Additionally, the impact of anatomical sites on fentanyl patch application was investigated. Due to the changes in skin layer thickness and skin temperature in different anatomical sites, the fentanyl uptake flux, fentanyl concentration, and pain intensity varied over different application locations. Based on our results, for a fentanyl patch with a nominal flux of 50 $\mu g/h$, the c_{max} for the patch applied on the chest, upper arm, and back is very similar and only varies for 1.7% and t_{max} varies for 3 h; however, the c_{max} for the flank is 15.3% more than the chest, and its t_{max} is 10.3 h less than the upper arm. This shows a high variation in the treatment outcomes between applying the fentanyl patch on the flank compared to the chest, back, and upper arm. Therefore, applying the same fentanyl patch on different body locations can lead to different therapy outcomes.

Furthermore, we conducted a study on the impact of seasonal changes and the patient's activity state on skin temperature, blood perfusion rate, and, eventually, the fentanyl uptake rate. In this regard, we considered an active and inactive state for the patient, with clothing suitable for the seasons (winter and summer). Based on our findings, the transition from an inactive state in winter to an active state in summer resulted in an increase of up to 11.8% in fentanyl uptake flux by capillaries, an increase of up to 4.3% in fentanyl concentration, and an increase of up to 4.9% in the minimum pain level. With greater changes in the conditions throughout different seasons, the changes in the outcomes can be more drastic.

Ultimately, we took into account the impact of temperature on fentanyl diffusion in order to control the fentanyl release to reach the target outcome of fentanyl therapy, which we considered a pain intensity of 3 on the VAS scale. In this way, the average

pain intensity (on the VAS scale) decreased from 5.44 to 4.12 from a no-heat condition to thermally enhanced delivery. The duration that the patient experienced mild pain intensity increased from 0h to 20.7 h. By implementing the thermally enhanced delivery of fentanyl, the standard deviation of c_{max} dropped from 0.08 to 0.05, and the average pain intensity standard deviation from 0.18 to 0.12. Therefore, not only did the thermally enhanced delivery of fentanyl improve pain relief, but it also reduced the variation in therapy outcomes throughout the treatment on different anatomical sites. Reducing therapy outcome variability leads to more predictable results, aiding physicians in patient treatment control.

Acknowledgments

This study received financial support from the OPO Foundation (grant "Digital human avatars help tailor transdermal pain management (TREATME)") and Margrit Weisheit Foundation and the Parrotia Foundation (grant titled "Digitale menschliche Avatare helfen bei der Anpassung der transdermalen Schmerztherapie in Echtzeit"). The funders had no role in the study's design, data collection, analysis, interpretation, preparation of this article, or the decision to submit it for publication.

References

1. Zaid Alkilani, A., McCrudden, M.T. and Donnelly, R.F., 2015. Transdermal drug delivery: Innovative pharmaceutical developments based on disruption of the barrier properties of the stratum corneum. Pharmaceutics, 7(4), pp.438-470.

2. Shingade GM. Review on: recent trend on transdermal drug delivery system. *J drug Deliv Ther*. 2012;2(1).

3. Tanwar H, Sachdeva R. Transdermal drug delivery system: A review. *Int J Pharm Sci Res*. 2016;7(6):2274.

4. Han Y, Yan W, Zheng Y, Khan MZ, Yuan K, Lu L. The rising crisis of illicit fentanyl use , overdose , and potential therapeutic strategies. *Transl Psychiatry*. 2019;(September 2018).

5. Wang D-D, Ma T-T, Zhu H-D, Peng C-B. Transdermal fentanyl for cancer pain: Trial sequential analysis of 3406 patients from 35 randomized controlled trials. *J Cancer Res Ther*. 2018;14(8):14.

6. Larsen RH, Nielsen F, Sørensen JA, Nielsen JB. Dermal Penetration of Fentanyl: Inter- and Intraindividual Variations. *Pharmacol Toxicol*. 2003;93(5):244-248.

7. Roy SD, Flynn GL. Transdermal Delivery of Narcotic Analgesics: pH, Anatomical, and Subject Influences on Cutaneous Permeability of Fentanyl and Sufentanil. *Pharm Res*. 1990;7(8):842-847.

8. Freise KJ, Newbound GC, Tudan C, Clark TP, Pharmacokinetics TP, Pharmaceuticals N. Pharmacokinetics and the effect of application site on a novel , long-acting transdermal fentanyl solution in healthy laboratory Beagles. 2012;35:27-33.

9. Defraeye T, Bahrami F, Ding L, Malini RI, Terrier A, Rossi RM. Predicting transdermal fentanyl delivery using mechanistic simulations for tailored therapy. *Front Pharmacol*. 2020;11.

10. Prodduturi S, Sadrieh N, Wokovich AM, Doub WH, Westenberger BJ, Buhse L. Transdermal delivery of fentanyl from matrix and reservoir systems: effect of heat and compromised skin. *J Pharm Sci*. 2010;99(5):2357-2366.

11. Zhang Q, Murawsky M, LaCount TD, et al. Evaluation of heat effects on fentanyl transdermal delivery systems using in vitro permeation and in vitro release methods. *J Pharm Sci*. 2020;109(10):3095-3104.

12. Dąbrowska AK, Spano F, Derler S, Adlhart C, Spencer ND, Rossi RM. The relationship between skin function, barrier properties, and body-dependent factors. *Ski Res Technol*. 2018;24(2):165-174.

13. Rim JE, Pinsky PM, Van Osdol WW. Multiscale modeling framework of transdermal drug delivery. *Ann Biomed Eng*. 2009;37(6):1217-1229.

14. Otto DP, De Villiers MM. The experimental evaluation and molecular dynamics simulation of a heat-enhanced transdermal delivery system. *AAPS PharmSciTech*. 2013;14(1):111-120.

15. Faulkner C, de Leeuw NH. Predicting the membrane permeability of fentanyl and its analogues by molecular dynamics simulations. *J Phys Chem B*. 2021;125(30):8443-8449.

16. Naegel A, Heisig M, Wittum G. Detailed modeling of skin penetration-An overview. *Adv Drug Deliv Rev*. 2013;65(2):191-207.

17. Walicka A, Iwanowska-Chomiak B. Drug diffusion transport through human skin. *Int J Appl Mech Eng*. 2018;23(4):977-988.

18. Anissimov YG, Jepps OG, Dancik Y, Roberts MS. Mathematical and pharmacokinetic modelling of epidermal and dermal transport processes. *Adv Drug Deliv Rev*. 2013;65(2):169-190.

19. Iordanskii AL, Feldstein MM, Markin VS, Hadgraft J, Plate NA. Modeling of the drug delivery from a hydrophilic transdermal therapeutic system across polymer membrane. *Eur J Pharm Biopharm*. 2000;49(3):287-293.

20. Defraeye, T., Bahrami, F. and Rossi, R.M., 2021. Inverse mechanistic modeling of transdermal drug delivery for fast identification of optimal model parameters. *Frontiers in Pharmacology*, *12*, p.641111.

21. Bahrami F, Rossi RM, De Nys K, Defraeye T. An individualized digital twin of a patient for transdermal fentanyl therapy for chronic pain management. *Drug Deliv Transl Res*. 2023:1-14.

22. Bahrami F, Rossi RM, Defraeye T. Predicting transdermal fentanyl delivery using physics-based simulations for tailored therapy based on the age. *Drug Deliv*. 2022;29(1):950-969.

23. Sameeh M, Elsaid A. Chebyshev collocation method for an interface parabolic partial differential equation model of transdermal medication delivery and transcutaneous absorption. *Partial Differ Equations Appl Math*. 2023;8:100582.

24. Björkman S. Reduction and Lumping of Physiologically Based Pharmacokinetic Models: Prediction of the Disposition of Fentanyl and Pethidine in Humans by Successively Simplified Models. *J Pharmacokinet Pharmacodyn*. 2003;30(4):285-307. doi:10.1023/A:1026194618660

25. Madden JC, Pawar G, Cronin MTD, Webb S, Tan YM, Paini A. In silico resources to assist in the development and evaluation of physiologically-based kinetic models. *Comput Toxicol*. 2019;11(February):33-49.

26. Pan S, Duffull SB. Automated proper lumping for simplification of linear physiologically based pharmacokinetic systems. *J Pharmacokinet Pharmacodyn*. 2019;46(4):361-370.

27. Shenoy P, Rao M, Chokkadi S, Bhatnagar S, Salins N. Developing mathematical models to compare and analyse the pharmacokinetics of morphine and fentanyl. *Indian J Anaesth*. 2024;68(1):111-117.

28. Rajoli RKR, Flexner C, Chiong J, et al. Modelling the intradermal delivery of microneedle array patches for long-acting antiretrovirals using PBPK. *Eur J Pharm Biopharm*. 2019;144:101-109.

29. Yan Q, Shen S, Wang Y, et al. The finite element analysis research on microneedle design strategy and transdermal drug delivery system. *Pharmaceutics*. 2022;14(8):1625.

30. Filipovic N, Saveljic I, Rac V, Olalde B, Bijelic G. Computational and experimental model of transdermal iontophorethic drug delivery system. *Int J Pharm*. 2017;533(2):383-388.

31. Corey B, Li A, Asrani R, D'Ambra R. A computational model for the facilitated transport of metronidazole by iontophoresis. 2012.

32. La Count TD, Zhang Q, Murawsky M, et al. Evaluation of heat effects on transdermal nicotine delivery in vitro and in silico using heat-enhanced transport model analysis. *AAPS J*. 2020;22:1-14.

33. Lacount TD, Zhang Q, Hao J, et al. Modeling Temperature-Dependent Dermal Absorption and Clearance for Transdermal and Topical Drug Applications. 2020:1-13.

34. Miller GE. Chapter 14 - Biomedical Transport Processes. In: Enderle JD, Bronzino JD, eds. *Introduction to Biomedical Engineering (Third Edition)*. Third Edition. Biomedical Engineering. Boston: Academic Press; 2012:937-993.

35. Rahman MS, Haque MA. Mathematical modeling of blood flow. In: *2012 International Conference on Informatics, Electronics & Vision (ICIEV)*. IEEE; 2012:672-676.

36. Fullstone G, Wood J, Holcombe M, Battaglia G. Modelling the transport of nanoparticles under blood flow using an agent-based approach. *Sci Rep*. 2015;5:1-13.

37. Siebert MW, Fodor PS. Newtonian and non-newtonian blood flow over a backward-facing step–a case study. In: *Proceedings of the COMSOL Conference, Boston*. Vol 27. ; 2009.

38. Fagrell B, Fronek A, Intaglietta M. A microscope-television system for studying flow velocity in human skin capillaries. *Am J Physiol Circ Physiol*. 1977;233(2):H318-H321.

39. Petrofsky JS. Resting blood flow in the skin: does it exist, and what is the influence of temperature, aging, and diabetes? *J Diabetes Sci Technol*. 2012;6(3):674-685.

40. Vuksanović V, Sheppard LW, Stefanovska A. Nonlinear relationship between level of blood flow and skin temperature for different dynamics of temperature change. *Biophys J*. 2008;94(10):L78-L80.

41. Defraeye T, Bahrami F, Ding L, Malini RI, Terrier A, Rossi RM. Predicting Transdermal Fentanyl Delivery Using Mechanistic Simulations for Tailored

Therapy. *Front Pharmacol*. 2020;11.

42. Marier JF, Lor M, Potvin D, DiMarco M, Morelli G, Sædder EA. Pharmacokinetics, tolerability, and performance of a novel matrix transdermal delivery system of fentanyl relative to the commercially available reservoir formulation in healthy subjects. *J Clin Pharmacol*. 2006;46(6):642-653.

43. Felmlee MA, Morris ME, Mager DE. Mechanism-based pharmacodynamic modeling. *Comput Toxicol Vol I*. 2012:583-600.

44. Gupta SK, Southam M, Gale R, Hwang SS. System functionality and physicochemical model of fentanyl transdermal system. *J Pain Symptom Manage*. 1992;7(3):S17-S26.

45. Karin Homber, Janay Kong, Sarah Lee and JH. the Effects of Applied Local Heat on Transdermal Drug Delivery Systems. 2008.

46. Nie S, Zhang C, Song J. Thermal management of epidermal electronic devices/skin system considering insensible sweating. *Sci Rep*. 2018;8(1):14121.

47. Umishio W, Ikaga T, Kario K, et al. Impact of indoor temperature instability on diurnal and day-by-day variability of home blood pressure in winter: a nationwide Smart Wellness Housing survey in Japan. *Hypertens Res*. 2021;44(11):1406-1416.

48. Li H, Hu T, Jia W, et al. Evaluation of Policy Influence on Long-Term Indoor Air Quality in Emperor Qin's Terra-Cotta Museum, China. *Atmosphere (Basel)*. 2015;6(4):474-489.

49. Fiala D, Lomas KJ, Stohrer M. A computer model of human thermoregulation for a wide range of environmental conditions: the passive system. *J Appl Physiol*. 1999;87(5):1957-1972.

50. Fiala D, Lomas KJ, Stohrer M. Computer prediction of human thermoregulatory and temperature responses to a wide range of environmental conditions. *Int J Biometeorol*. 2001;45:143-159.

51. Koelblen B, Psikuta A, Bogdan A, Annaheim S, Rossi RM. Thermal sensation models: Validation and sensitivity towards thermo-physiological parameters. *Build Environ*. 2018;130:200-211.

52. Martínez N, Psikuta A, Kuklane K, et al. Validation of the thermophysiological model by Fiala for prediction of local skin temperatures. *Int J Biometeorol*. 2016;60:1969-1982.

53. Psikuta A, Fiala D, Laschewski G, et al. Validation of the Fiala multi-node thermophysiological model for UTCI application. *Int J Biometeorol*. 2012;56:443-460.

54. Fojtlín M, Psikuta A, Fišer J, Toma R, Annaheim S, Jícha M. Local clothing properties for thermo-physiological modelling: comparison of methods and body positions. *Build Environ*. 2019;155:376-388.

55. Wienert V, Sick H, Zur Mühlen J. Local thermal stress tolerance of human skin. *Anasth Intensivther Notfallmed*. 1983;18(2):88-90.

56. Greene LC, Hardy JD. Spatial summation of pain. *J Appl Physiol*. 1958;13(3):457-464.

57. Ong BB, Milne N. Injury, fatal and nonfatal: burns and scalds. 2016.

58. Lee CM, Jin S-P, Doh EJ, Lee DH, Chung JH. Regional variation of human skin surface temperature. *Ann Dermatol*. 2019;31(3):349-352.

59. Shomaker TS, Zhang J, Ashburn MA. Assessing the impact of heat on the systemic delivery of fentanyl through the transdermal fentanyl delivery system. *Pain Med*. 2000;1(3):225-230.

60. Dai C, Zhang H, Arens E, Lian Z. Machine learning approaches to predict thermal demands using skin temperatures: Steady-state conditions. *Build Environ*. 2017;114:1-10.

61. Lee Y, Hwang K. Skin thickness of Korean adults. *Surg Radiol Anat*. 2002;24(3-4):183.

62. Yang X, Cui Y, Yue J, et al. The histological characteristics, age-related thickness change of skin, and expression of the HSPs in the skin during hair cycle in yak (Bos grunniens). *PLoS One*. 2017;12(5):e0176451.

63. Rim JE, Pinsky PM, Van Osdol WW. Finite element modeling of coupled diffusion with partitioning in transdermal drug delivery. *Ann Biomed Eng*. 2005;33(10):1422-1438.

64. Neerken S, Lucassen GW, Bisschop MA, Lenderink E, Nuijs T (A. M. Characterization of age-related effects in human skin: A comparative study that applies confocal laser scanning microscopy and optical coherence tomography. *J Biomed Opt*. 2004;9(2):274.

65. Braverman IM. The Cutaneous Microcirculation. *J Investig Dermatology Symp Proc*. 2000;5(1):3-9.

66. Micali G, Verzì AE, Musumeci ML, Nardone B, Monfrecola G, Lacarrubba F. Noninvasive Evaluation of Diameter and Density of Dermal Papillae in Psoriatic and Healthy Skin Using Reflectance Confocal Microscopy: An Intrapatient Controlled Study and a Review. *J Invest Dermatol*. 2023;143(4):667-669.e2.

67. Parazynski SE, Tucker BJ, Aratow M, Crenshaw A, Hargens AR. Direct measurement of capillary blood pressure in the human lip. *J Appl Physiol*. 1993;74(2):946-950.

68. Nader E, Skinner S, Romana M, et al. Blood rheology: key parameters, impact on blood flow, role in sickle cell disease and effects of exercise. *Front Physiol*. 2019;10:1329.

69. Bjorkman S, Wada RD, Stanski D. Application of physiologic models to predict the influence of changes in body composition and blood flows on the pharmacokinetics of fentanyl and alfentanil in patients. *Anesthesiol J Am Soc Anesthesiol*. 1998;88(3):657-667.

70. Miller RS, Peterson GM, McLean S, Möller C. Effect of cardiopulmonary bypass on the plasma concentrations of fentanyl and alcuronium. *J Clin Pharm Ther*. 1997;22(3):197-205.

71. Encinas E, Calvo R, Lukas JC, Vozmediano V, Rodriguez M, Suarez E. A predictive pharmacokinetic/pharmacodynamic model of fentanyl for analgesia/sedation in neonates based on a semi-physiologic approach. *Pediatr Drugs*. 2013;15(3):247-257.

72. Fu M, Weng W, Yuan H. Numerical simulation of the effects of blood perfusion, water diffusion, and vaporization on the skin temperature and burn injuries. *Numer Heat Transf Part A Appl*. 2014;65(12):1187-1203.

73. Guangfa G, Shujie Y, Ruiyuan H, Yongchi L. Experimental investigation on thermal physical properties of an advanced polyester material. *Phys Procedia*. 2012;25:333-338.

74. Reis JML dos, Cardoso JL. Mechanical properties of recycled Kraft paper residue polyester composites. *Mater Res*. 2014;17:888-892.

75. Johnson NN, Abraham JP, Helgeson ZI, Minkowycz WJ, Sparrow EM. An archive of skin-layer thicknesses and properties and calculations of scald burns with comparisons to experimental observations. 2011.

76. Xu F, Seffen KA, Lu TJ. Non-Fourier analysis of skin biothermomechanics. *Int J Heat Mass Transf*. 2008;51(9-10):2237-2259.

77. Nahirnyak VM, Yoon SW, Holland CK. Acousto-mechanical and thermal properties of clotted blood. *J Acoust Soc Am*. 2006;119(6):3766-3772.

78. Mishra D, Dehury J, Rout L, Satapathy A. The effect of particle size, mixing conditions and agglomerates on thermal conductivity of BN-polyester & multi-sized BN-hybrid composites for use in micro-electronics. *Mater Today Proc*. 2020;26:3187-3192.

79. US Food and Drug Administration. Duragesic Label. 2005.

80. Prausnitz, M.R. and Langer, R., 2008. Transdermal drug delivery. *Nature bio-technology*, *26*(11), pp.1261-1268.

Graphical Abstract